metals

MDPI

Article

Evaluation of Primary Water Stress Corrosion Cracking Resistance of Three Heats of Alloy 600 in 400 °C Hydrogenated Steam Condition

Eunsub Yun [1,2], Hansub Chung [1] and Changheui Jang [2,*]

[1] Central Research Institute, Korea Hydro and Nuclear Co., Ltd., 70, 1312-gil, Yuseong-daero, Yuseong-gu, Daejeon 34101, Korea; eunsub.yun@khnp.co.kr (E.Y.); hansubchung@khnp.co.kr (H.C.)

[2] Department of Nuclear and Quantum Engineering, Korea Advanced Institute of Science and Technology, 291 Daehak-ro, Yuseong-gu, Daejeon 34141, Korea

* Correspondence: chjang@kaist.ac.kr; Tel.: +81-42-350-3824

Received: 6 December 2017; Accepted: 5 February 2018; Published: 12 February 2018

Abstract: For Alloy 600, primary water stress corrosion cracking (PWSCC) is one of the key material degradation mechanisms in pressurized water reactors (PWRs). To identify the governing factors of PWSCC resistance, a systematic investigation into the role of each factor was performed. A PWSCC initiation test was performed for 3 heats of Alloy 600 in the 400 °C hydrogenated steam condition. Based on the test results, the effects of known factors like chemical composition, mechanical strength, grain boundary carbide coverage, grain boundary character, and surface cold work on PWSCC resistance were discussed. In addition, surface oxide morphology and penetrative oxide depth was compared. From this study, grain boundary character was considered to be the most dominant factor affecting the PWSCC resistance.

Keywords: Alloy 600; primary water stress corrosion cracking; hydrogenated steam; grain boundary character

1. Introduction

Alloy 600, a Ni-Cr-Fe alloy, is widely used as the pressure boundary component of pressurized water reactors (PWRs), such as steam generator tubes and penetration nozzles. It has good mechanical strength and excellent corrosion resistance in PWR operating environments. However, the occurrence of primary water stress corrosion cracking (PWSCC) has been widely reported worldwide in the PWR fleet as the operating year increases [1].

Several factors affecting Alloy 600 PWSCC susceptibility have been suggested. For example, chemical compositions like those of nickel and chromium are known to affect the PWSCC susceptibility of Ni-Cr-Fe alloys. It has been reported that high nickel concentration above about 70 wt% showed high PWSCC susceptibility in pure water conditions [2]. Chromium is certainly beneficial to PWSCC resistance [3], and Alloy 690, which has higher chromium concentration than Alloy 600, is used as the replacement material of Alloy 600 components in PWRs. Meanwhile, heat treatment condition, microstructure, and yield strength are interrelated in several ways. Grain sizes are affected by cool down rate after solution annealing. Alloys with smaller grain would show higher yield strength, which in turn would result in shorter PWSCC initiation time [4]. Slow cooling rates after annealing would precipitate more carbides in the grain boundary [5], and the presence of grain boundary carbides is known to increase the PWSCC resistance [3]. Dissolved hydrogen concentration has significant effect on the PWSCC resistance of Alloy 600 such that PWSCC resistance can be explained by the hydrogen fugacity and Ni/NiO equilibrium [6,7]. However, due to the complexity of the inter-relationship among the above mentioned factors, it is difficult to identify the dominant factors affecting the PWSCC

susceptibility of Alloy 600. This could be the reason that the suggested PWSCC mechanisms, such as internal oxidation, hydrogen embrittlement, and film rupture models, were not able to explain all the PWSCC dependencies with those factors [8–12].

In the laboratory, it is usual to do the PWSCC test at the accelerated condition. However, to utilize the test results for the life assessment of the Alloy 600 components, the accelerated test conditions should not alter that PWSCC characteristics and factor could be correlated by quantitative measure. PWSCC initiation time was known to have an inverse power law dependence on the applied stress, with an exponent of 4–5 for Alloy 600 and its weld materials [13,14], thus significantly shortening the PWSCC initiation time by applying high stress during the test. Also, the PWSCC initiation time could be expressed as a function of temperature in an Arrhenius equation with activation energy of 180~209 kJ/mol [13–15]. Many tests are performed at or below the 360 °C due to the concern of the continuity of corrosion mechanisms in steam environment. However, detailed oxide layer investigation showed that similar characteristics existed between the sub-cooled water and superheated steam [16]. Therefore, the accelerated test can be performed while maintaining a similar oxide characteristic under high-temperature steam condition.

In this work, a PWSCC initiation test was conducted with constant deflected specimens in 400 °C hydrogenated steam conditions for 3 heats of Alloy 600 with different product forms. Crack initiation time was measured by visual and destructive examination. Then, the factors affecting different PWSCC susceptibility were quantitatively evaluated and compared with the test results to identify the dominant factors. In addition, the surface oxide morphology and oxide penetration were analyzed and the implication on internal oxidation was discussed.

2. Materials and Methods

2.1. Materials and Test Specimen

Three commercial heats of Alloy 600, whose composition is shown in Table 1, were used for this study. The first heat, specified as 'Tube', was provided by a nuclear component manufacturer in a tube form with 19.05 mm outside diameter and 1.09 mm thickness. The heat treatment condition of 'Tube' is mill-annealed at 1024 °C for 4 min. The second heat was 'Rod' with 120 mm diameter provided by commercial supplier in annealed condition. The third heat was 'Plate' with 50 mm thickness provided in annealed and hot rolled condition. For 'Rod' and 'Plate', the detailed heat treatment condition was not provided. Nonetheless, the mechanical properties shown in Table 2 satisfy the relevant ASTM (American Society for Testing and Materials) specification. The data shown in Tables 1 and 2 are from the suppliers, as the analysis and measured data by authors showed similar results except the tensile properties of 'Tube', which were not measured. Figure 1 shows the microstructure of 'Tube', 'Rod' and 'Plate'. 'Tube' and 'Rod' have an equiaxed microstructure, but 'Plate' has a different microstructure depending on the direction, showing a banded structure in planes normal to the rolling direction (T and S in Figure 1c).

Table 1. Chemical composition of Alloy 600 heats used in the study (in wt%).

Heat	C	Mn	Si	Ni	Cr	Cu	Fe	P	S
Tube	0.023	0.19	0.22	75.82	15.25	0.19	8.04	0.01	<0.001
Rod	0.04	0.53	0.48	72.10	16.04	0.05	10.00	-	0.001
Plate	0.05	0.26	0.22	74.2	16.08	0.02	8.99	0.01	<0.001

Table 2. Mechanical properties and grain size of Alloy 600 heats used in the study.

Heat	Yield Strength (0.2% Offset, MPa)	Tensile Strength (MPa)	Elongation (%)	Grain Size No.
Tube	248	614	-	5
Rod	257	584	46	6.1
Plate	275	645	41	4.5

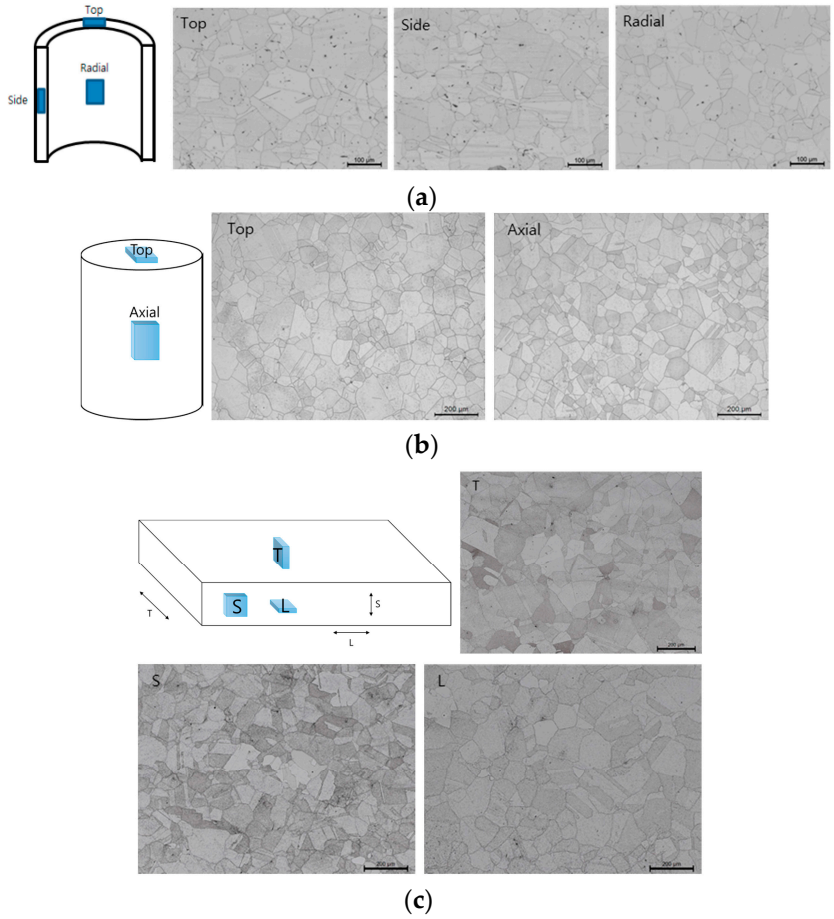

Figure 1. Microstructure of three heats of Alloy 600. (**a**) 'Tube'; (**b**) 'Rod'; (**c**) 'Plate'.

Ovalized tube (OT) specimen is used for PWSCC initiation test (KLES, Daejeon, Korea). Figure 2 shows the fabrication process of the OT specimens. Tubes are compressively deformed by about 1/3 of the tube diameter, then rotated by 90° and deformed again to reach their original diameter. 'Tube' was used as-is, 'Rod' and 'Plate' were lathe machined into tube shapes. Figure 3 shows the orientation of OT specimen for the 'Rod' and 'Plate' heats. Finally, specimens were bolted between 6~12 mm thick stainless steel plates to maintain stress. The linear surface roughness in the axial direction (perpendicular to the milling direction) was measured to be about Ra = 0.27 μm and 0.48 μm for 'Tube' and 'Rod'/'Plate', respectively. For lathes machined 'Rod' and 'Plate' specimens, about 100 μm thick cold worked layer was identified by Micro Vickers hardness test (Mitutoyo, Kawasaki, Kanagawa Prefecture, Japan).

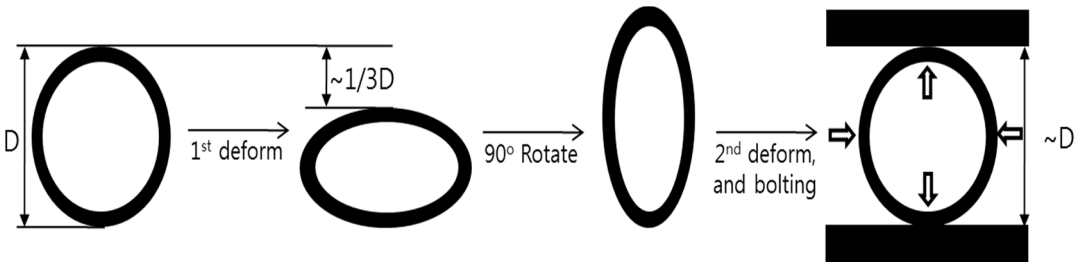

Figure 2. Fabrication process of ovalized tube (OT) specimen.

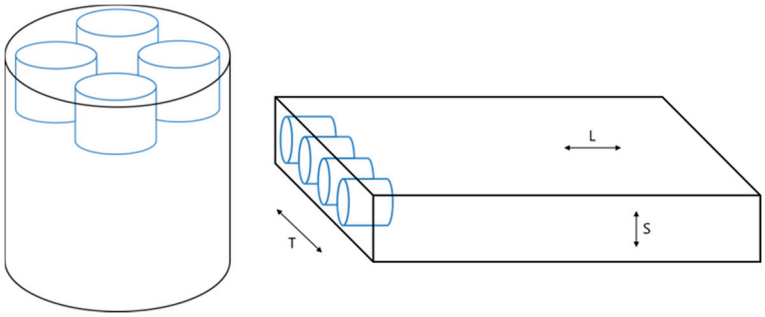

Figure 3. Orientation of OT specimens for 'Rod' and 'Plate' heats.

The advantage of OT specimens is that high tensile stress is developed at the narrow region of inside diameter and outside diameter as shown in arrow of Figure 2. Three different sizes of OT specimens were used for this study. Table 3 shows the size and the deformed distance of the OT specimens.

Table 3. Dimensions of ovalized tube (OT) specimens.

Specimen	Outside Diameter (mm)	Thickness (mm)	Length (mm)	Deformed Distance (mm, 1st/2nd)	Note
19OT	19.05	1.09	35	7/~5	'Tube'
35OT	35	2.5	35	11/~8	'Rod' and 'Plate'
45OT	45	3.2	45	15/~11	'Rod' and 'Plate'

For the bolted OT specimens, applied stress was calculated by finite element method (FEM) analysis using ABAQUS (Dassault systemes, Ver. 6.10, Paris, France). Figure 4 shows the FEM model and simulation steps. The results showed that about 1040 and 630 MPa peak circumferential stress are developed on the inside surface (ID) and the outside surface (OD) of the bolted OT specimen at room temperature. It should be noted that for the FEM analysis, surface cold worked region was not considered. To confirm the calculated stress values, applied stress on the outside surface of the 45OT specimen of 'Plate' was measured using X-ray technique by MSF-3M (Rigaku, Tokyo, Japan) with 30 kV and 10 mA condition using Cr target. Before measurement, up to 130 μm was removed from the specimen surface by electro etching to remove the cold worked area. For the specimen with less than 60 μm removed, the measured stress was over 870 MPa, which was greater than FEM calculated value of 630 MPa. For the specimen with 60 μm removed, the measured value was 654 ± 30 MPa, which was very similar to the calculated value. For the specimen with 130 μm removed, the measured value was 463 ± 57 MPa, less than the calculated value. The measured stress could be considered as the stress at the location because the penetration depth of X-ray is about 5 μm [17]. Highly measured stress is probably due to the 100 μm thick cold worked layer. Meanwhile, stress at 130 μm depth was a little far from the expected value. It could be explained by combined effect of stress release by the deep electro etching and decreasing stress trend along the depth direction. Then, the applied stress at the test temperature of 400 °C was calculated using the same FEM model, and the results showed that the peak circumferential tensile stress on the inside surface were 880 and 480 MPa, respectively.

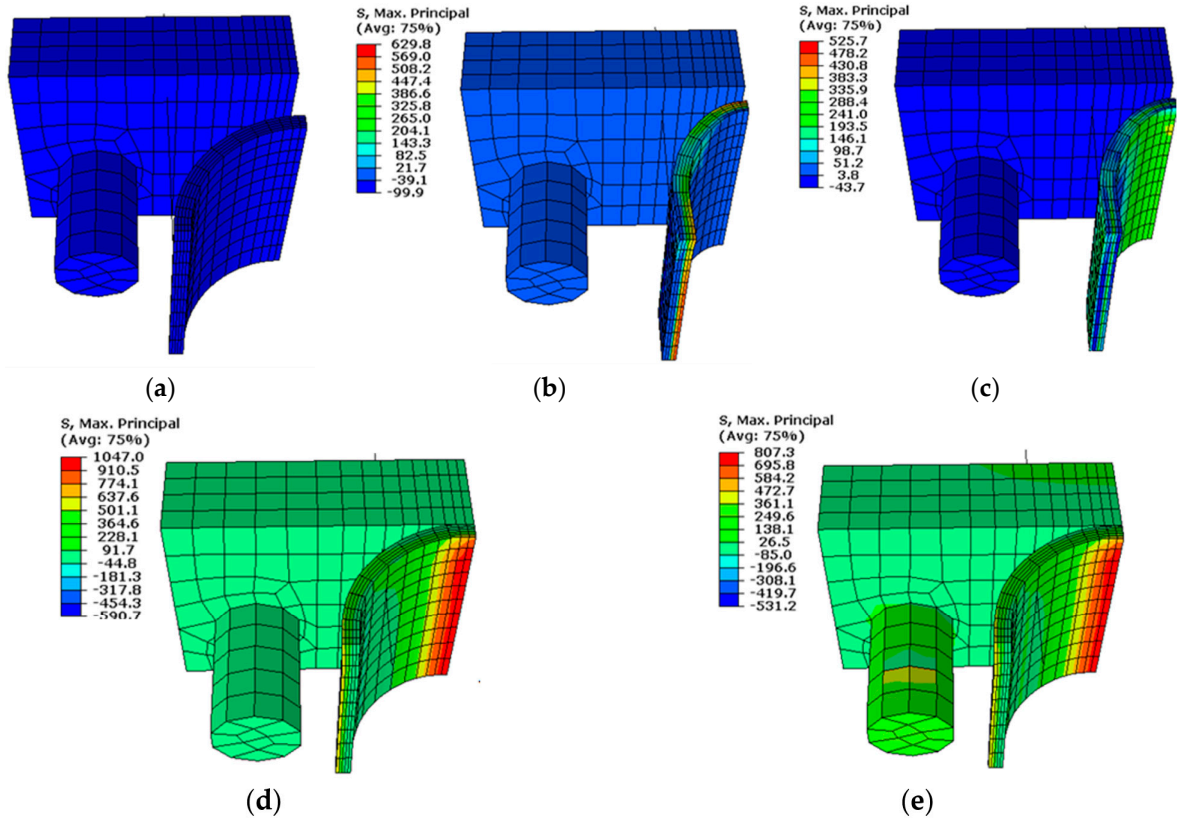

Figure 4. FEM simulation step. (**a**) Initial; (**b**) 1st deform; (**c**) Release; (**d**) 2nd deform; (**e**) Heat up to 400 °C.

2.2. PWSCC Test

Bolted OT specimens were installed in the static autoclave at 15 MPa, 400 °C with hydrogenated steam conditions. High-pressure hydrogen gas was directly injected into the autoclave to maintain hydrogen partial pressure at 56 kPa, which is known to maintain the Ni/NiO transition condition at 400 °C [18]. Pd-Ag tube was inserted into the autoclave to monitor the hydrogen partial pressure during the test.

Initially, 500 h immersion test was performed for multiple 'Tube', 'Rod', and 'Plate' specimens. Then short-term supplementary tests were performed for more susceptible heats ('Tube and 'Rod'). Both short-term and longer-term (up to 800 h) tests were performed for less susceptible heat ('Plate'). Crack initiation was investigated by a low-magnification optical microscope for all specimens immersed for certain test period. If a crack is identified, the specimen is removed from the autoclave for further analysis. The un-cracked ones are returned to the autoclave if longer-term exposure is needed. The final PWSCC initiation test matrix is summarized in Table 4.

Table 4. Summary of PWSCC initiation test expressed as '# of specimens with crack/# of tested specimens'. The measured maximum crack depths as a fraction of thickness are also shown.

Test Time	100 h	200 h	300 h	500 h [1]	700 h	800 h
Tube	2/2 (ID: 6.6%, OD: 2.0%)	2/2 (ID: 17.0%, OD: 15.1%)	-	2/2 (ID: 44.7%, OD: 22.2%)	-	-
Rod	4/5 (ID: 10.4%, OD: 4.2%)	-	-	6/6 (ID: 45.6%, OD: 84.7%)	-	-
Plate	0/8	0/6	0/6	1/10 (ID [2])	3/6 (ID: 27.4%, OD: 12.9%)	2/2 (ID [3], OD [3])

[1] This test was performed first to evaluate the PWSCC resistance of 3 heats of Alloy 600; [2] Crack depth could not be measured, as crack was too shallow; [3] Crack depth was not measured.

Optical microscope (DMi8 A, LEICA, Wetzlar, Land Hessen, Germany), Scanning electron microscope (SEM, 7100F, JEOL, Tokyo, Japan), Focused ion beam (FIB, Helios G4 UX, Thermo Fisher Scientific, Waltham, MA, USA) and electron back scattered diffraction (EBSD, Nordlys Nano, Oxford Instruments, Abingdon, Oxfordshire, UK) were used for oxide layer and crack investigation.

3. Results and Discussion

3.1. PWSCC Initiation Test Results

The PWSCC test results are summarized in Table 4. The 'number of specimens with cracks/number of tested specimens' and the measured maximum crack depths at ID and OD of the cracked specimens as a fraction of specimen thickness are also shown in Table 4. As shown in Table 4, cracks were detected for most of the specimen for both 'Tube' and 'Rod' specimens as early as 100 h exposure, while none of 'Plate' showed cracking until 300 h exposure. In the case of 'Plate', only 1 out of 10 specimens showed cracks after 500 h exposure, and it took 800 h exposure to fail all specimens. Generally, multiple cracks were detected at ID and OD of the cracked specimen. The only exception was a very shallow single crack found at the ID of the 1 'Plate' specimen after 500 h exposure, which was considered 'cracked' for the sake of conservatism. For most of cracked "Tube" and 'Plate', the fractional crack depth was greater at ID (where applied stress was higher) than at OD (where applied stress was lower), and became greater as exposure time increased. These results indicate that 'Tube' and 'Rod' heats are more susceptible to PWSCC than the 'Plate' heat.

The cross-section of the cracked specimens cut and etched using 2% bromine solution for grain boundary observation. The SEM photos of the 'Rod' specimen cracked after 100 h exposure are shown in Figure 5. All cracks were developed through the grain boundary, suggesting the cracking mechanism is inter-granular stress corrosion cracking (IGSCC). In Figure 5a, multiple cracks with different depths are shown. For these cracks, cracks stopped in front of the grain boundary carbide (Figure 5b,c), which acted as a barrier for crack growth. However, some cracks could overcome the barrier and grow beyond the grain boundary carbide, which would leave the partially broken and by-passed morphology as shown in Figure 5e. That is, when the crack grows far enough from the carbide, additional tensile stress induced by crack opening could be high enough to detach or break the carbides from the grain boundary.

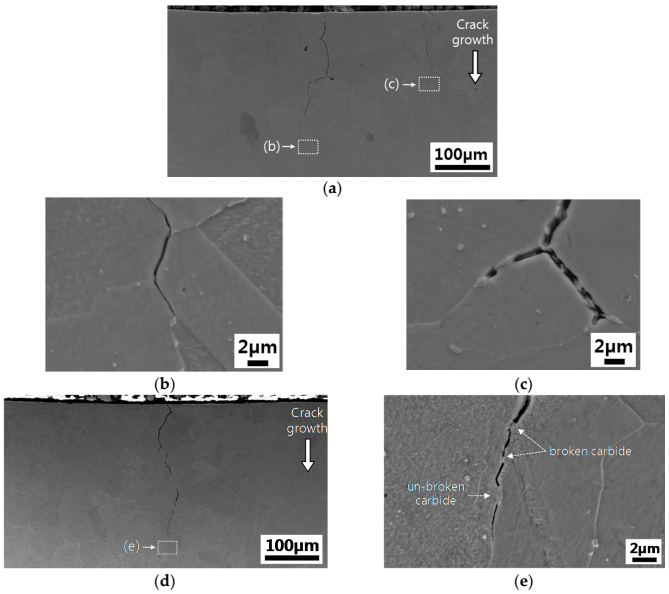

Figure 5. SEM photos of cracks found at the ID surface of 'Rod' specimen after 100 h exposure: (**a**) Low magnification photo of crack; (**b**) Enlarged photos of left crack tips in (**a**); (**c**) Enlarged photos of right crack tips in (**a**); (**d**) Low magnification photo of crack; (**e**) enlarged photos of crack tips in (**d**).

3.2. Factors Affecting the PWSCC Initiation

In this section, the PWSCC test results shown in Table 4 are discussed in view of the applicability of key factors that have been proposed to affect the PWSCC initiation of Alloy 600. First, Cr is known as the most important factor affecting the PWSCC susceptibility of Ni-Cr-Fe alloys such that SCC resistance increases as the Cr contents decreases [3]. In this study, 'Tube' has lower Cr contents than the 'Rod' and 'Plate' (Table 1). However the difference in Cr contents is about 0.8 wt%, which is not significant for seeing the effect on PWSCC susceptibility among the tested Alloy 600 heats.

Yield strength is considered one of the important factors affecting SCC susceptibility. For example, Daret et al. [4] reported that the crack initiation time decreased as the yield strength increased as following equation.

$$t_i = 1.5 \times 10^6 \, YS_{RT}{}^{-1.8} \quad (1)$$

where, t_i = crack initiation period (hour)

YS_{RT} = yield strength at room temperature.

Thus, heats with higher yield stress are expected to be more susceptible to PWSCC showing shorter crack initiation time. Among the Alloy 600 heats tested, 'Plate' showed somewhat higher yield strength than the others. However, 'Plate' was much less susceptible to PWSCC, as mentioned in the previous section. Therefore, yield strength could not be considered an appropriate factor to explain the observed PWSCC resistance of tested Alloy 600 heats.

As mentioned in the previous section, grain boundary carbides would be beneficial for increasing the PWSCC resistance, as they act as barriers to crack growth. So, grain boundary carbide coverage was measured on more than 3 SEM photos for each heat, and the results are summarized in Table 5. 'Rod' showed the smallest grain boundary carbide coverage, and 'Tube' showed high grain boundary carbide coverage similar to 'Plate'. These observations are somewhat mixed, in that, despite similarly high grain boundary carbide coverage, 'Plate' was resistant to PWSCC while 'Tube' was far less resistant.

Table 5. Measured grain boundary carbide coverage.

Heat	Grain Boundary Carbide Coverage
Tube	47.1 ± 0.6%
Rod	39.6 ± 9.2%
Plate	51.5 ± 6.0%

In addition, grain boundary character were measured for each heat of Alloy 600 using EBSD, which adopted Brandon's criterion, as was used in similar studies [19–21]. Figure 6 shows the typical microstructure where random grain boundary boundaries are in black and ∑3 twin boundaries are in red lines. The quantitative analysis results of the grain boundary characters are summarized in Table 6. It has been reported that low angle boundary (<15°) and coincident-site lattice boundaries (CSLBs) are resistant to inter-granular stress corrosion cracking [19,20]. On the other hand, others have suggested that, among CSLBs, only ∑3 twin boundaries are crack-resistant [21]. It is shown in Figure 6d that for all 3 heats tested in this study, grain boundaries were mostly of high angle and there were very few low-angle boundaries (fewer than 6%, as shown in Table 6) were present. Therefore, the small difference in low-angle boundary fraction could not explain the hugely different PWSCC susceptibility observed. Meanwhile, there are some differences in CSLB and ∑3 boundary fractions among the 3 heats of Alloy 600, as shown in Table 6. Both CSLB and ∑3 boundary fractions were much smaller for 'Tube' and 'Rod' compared to 'Plate', whose grain boundaries were about 68% CSLB (or 61% ∑3 boundary). As the relative fraction of ∑3 boundary to CSLB was about the same for all 3 heats, either CSLB or ∑3 boundary fractions could be used as an indicator of the PWSCC resistance of Alloy 600.

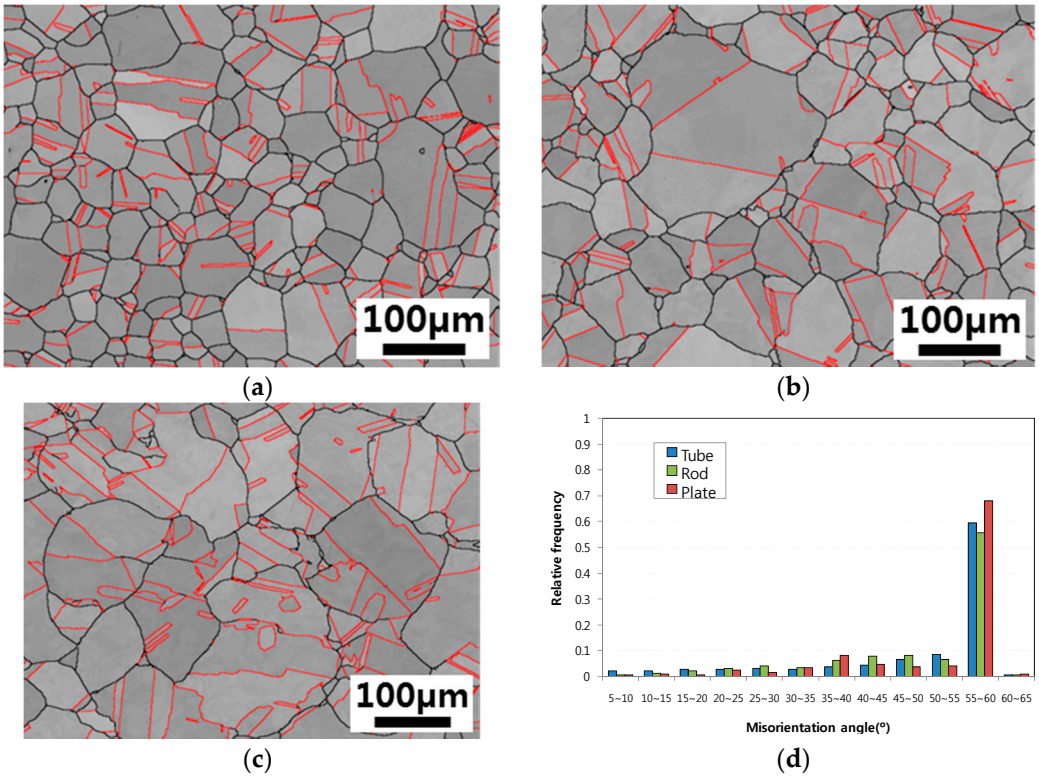

Figure 6. Grain boundary character analysis using EBSD where random boundaries are in black and twin boundaries are in red line: (**a**) Tube; (**b**) Rod; (**c**) Plate; (**d**) Grain boundary angle distribution plot.

Table 6. Fraction (%) for some important grain boundary characters.

Grain Boundary Character	Tube	Rod	Plate
Low angle boundary (<15°)	5.6	2.0	2.0
CSLB ($\sum \leq 29$)	48.2	52.2	68.2
$\sum 3$ boundary	43.3	46.7	60.7
$\sum 3$ boundary relative to all CSLB	89.9	89.6	88.9

All fractions are based on the length of boundaries.

As mentioned previously in specimen preparation, OT specimens for 'Rod' and 'Plate' were lathe machined and a cold-worked surface layer that was about 100 μm thick was present, while 'Tube' specimens were in annealed condition and the surface was free of cold work. Authors had concern that the presence of a surface cold-worked layer would increase PWSCC susceptibility of lathe-machined specimens. However, the test results indicated that the presence of surface cold-worked layer had no effect on PWSCC susceptibility such that 'Plate' with surface cold-worked layer showed much resistance to PWSCC, but 'Tube' that was free of a surface cold-worked layer was susceptible to PWSCC. The large deformation added to the specimens during the OT specimen fabrication process may have shadowed the pre-existing cold-worked layer.

3.3. Suraface Oxides and Oxygen Penetration

Surface oxides formed on the specimens tested for 100 h were observed by SEM. Figure 7 shows that the surface was mostly covered with very fine oxide particles of a few tens of nanometers for all 3 heats. However, blocky oxides of about 100 nm were found on the surface of 'Rod', while fine platelet oxides were found for 'Tube' and 'Plate'. It has been reported that the blocky oxides are Ni-Fe spinel oxides formed on top of Cr-rich oxide layer [22]. The presence of blocky oxides for 'Rod' could be

correlated with the relatively poor protection of underlying Cr-rich oxide layer as they are known to be formed by Ni-Fe diffusion through the oxide layer [23].

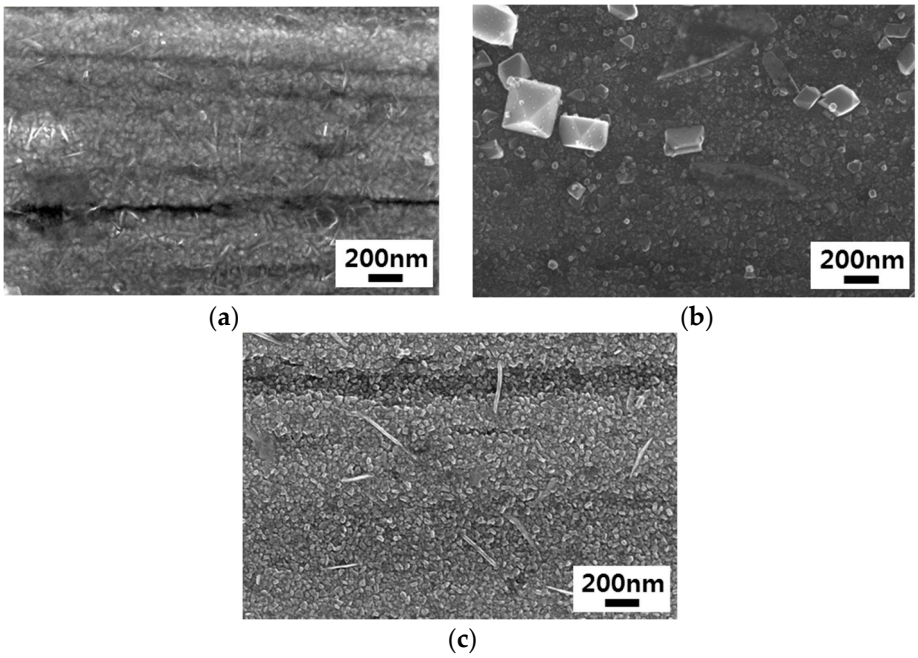

Figure 7. SEM image of surface oxides formed on the specimens tested for 100 h: (**a**) Tube; (**b**) Rod; (**c**) Plate.

Meanwhile, the cross-section images of the specimens tested for 100 h were observed by the FIB/SEM. As shown in Figure 8, penetrative chromium oxide was observed in some part (more than 75% of observed cross-section) of 'Tube' and 'Rod', while such penetrative oxide was not found in 'Plate'. This could be an indication of the better protectiveness of Cr-rich oxide layer formed on 'Plate'. The depth of penetrative oxide was several hundred nanometers for both 'Tube' and 'Rod', as shown in Figure 8. Others have also observed the penetrative oxides on Ni-Cr-Fe alloys susceptible to PWSCC [24–26]. For example, Lindsay et al. showed that grain boundary internal oxidation was deeper than penetrative oxide (or, intragranular oxide) for the Alloy 600, and when the former was less, the later decreased or was not present [24]. Also, Persaud et al. showed that grain boundary internal oxidation was deeper than intragranular oxides for the two heats of Alloy 600 [25]. Therefore, the presence of penetrative oxides could be correlated with the formation of internal oxidation of Alloy 600, such that penetrative oxides were found on top of bulk grains, while penetrative oxides gradually disappears near the grain boundary where significant internal oxidation was observed [26]. Therefore, the presence of penetrative oxides in 'Tube' and 'Rod' could be used as an indirect indication of the presence of internal oxidation, which is known to be the most probable PWSCC mechanism of Ni-Cr-Fe alloys. For direct comparison of the degree of internal oxidation among 3 heats of Alloy 600, more detailed analysis using transmission electron microscope is needed.

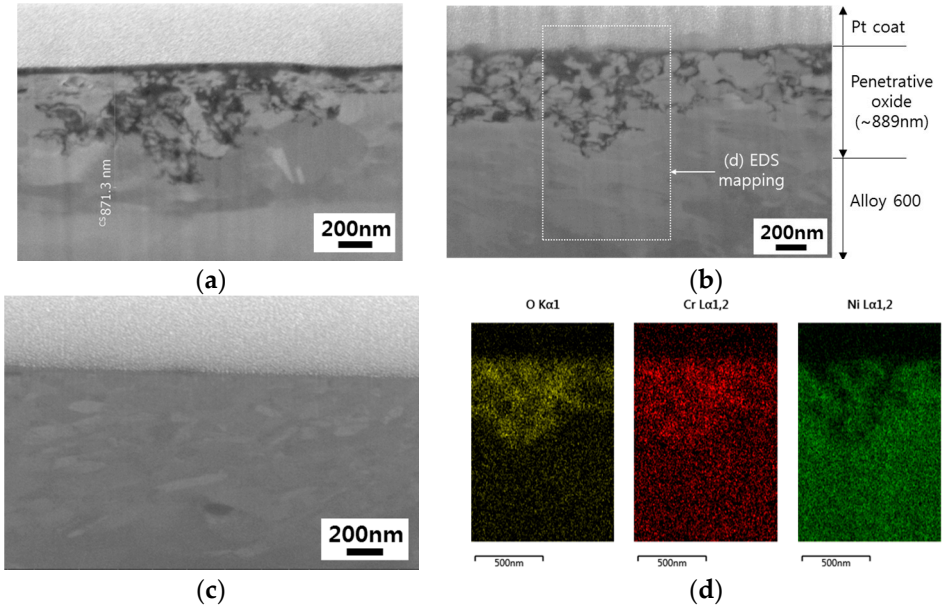

Figure 8. FIB/SEM images of cross-section near surface of the specimens tested for 100 h (38° tilted image, penetrative oxide depth were corrected by tilt angle): (**a**) Tube; (**b**) Rod; (**c**) Plate; (**d**) EDS mapping of area indicated in (**b**).

4. Conclusions

A PWSCC initiation test was performed for 3 heats of Alloy 600 in the 400 °C hydrogenated steam condition. Then the key factors affecting the PWSCC resistance were discussed while comparing the PWSCC initiation test results. Based on the test results and discussions, it was found that the grain boundary character was considered to be the most dominant factor affecting the PWSCC resistance. The effect of surface cold-worked was not observed in this study, possibly due to the OT specimen preparation process involving severe plastic deformation. In addition, the poor PWSCC resistance could be correlated with the presence of penetrative oxide caused by the poor protectiveness of surface Cr-rich oxide layer.

Acknowledgments: This study was funded by Electric Power Research Institute as a part of collaborative research with Korea Hydro & Nuclear Power Co. Ltd.

Author Contributions: E.Y. and H.C. conceived and designed the experiments; E.Y. performed the PWSCC experiment and investigated the specimens; H.C. and C.J. analyzed the data and contribute the discussion on the results; E.Y. wrote the paper; C.J. corrected the paper.

Conflicts of Interest: The authors declare no conflict of interest.

References

1. King, C.P. *PWSCC of Alloy 600 Type Materials in Non-Steam Generator Tubing Applications*; Product ID 1007832; EPRI: Palo Alto, CA, USA, 2002; pp. 1–2.
2. Staehle, R.W. Historical Views on Stress Corrosion Cracking of Nickel-Based Alloys: The Corious Effect. In *Stress Corrosion Cracking of Nickel-Based Alloys in Water-Cooled Nuclear Reactors*; Féron, D., Staehle, R.W., Eds.; Elsevier: Amsterdam, The Netherlands, 2016; p. 15. ISBN 978-0-08-100062-5.
3. Yonezawa, T. Methodology to Understand the Mechanisms of PWSCC. In Proceedings of the 9th International Symposium on Environmental Degradation of Materials in Nuclear Power Systems—Water Reactors, Newport Beach, CA, USA, 1–5 August 1999; pp. 15–19.
4. Daret, J. Initiation of SCC in Alloy 600 Wrought Materials: A Laboratory and Statistical Evaluation. In Proceedings of the 12th International Conference on Environmental Degradation of Materials in Nuclear Power System—Water Reactors, Salt Lake City, UT, USA, 14–18 August 2005; pp. 937–944.

5. Fyfitch, S. Corrosion and Stress Corrosion Cracking of Ni-Base Alloys. In *Comprehensive Nuclear Materials*; Konings, R.J.M., Allen, T.R., Stoller, R., Yamanaka, S., Eds.; Elsevier: Amsterdam, The Netherlands, 2012; pp. 75–88. ISBN 978-0-08-056027-4.
6. Dozaki, K.; Akutagawa, D.; Nagata, N.; Takiguchi, H.; Norring, K. Effects of Dissolved Hydrogen Content in PWR Primary Water on PWSCC Initiation Property. *E-J. Adv. Maint.* **2010**, *2*, 65–76.
7. Andresen, P.L.; Hickling, J.; Ahluwalia, A.; Wilson, J. Effect of Hydrogen on Stress Corrosion Crack Growth Rate of Nickel Alloys in High-Temperature Water. *Corrosion* **2008**, *64*, 707–720. [CrossRef]
8. Scott, P.M.; le Calvar, M. Some possible mechanisms of intergranular stress corrosion cracking of Alloy 600 in PWR primary water. In Proceedings of the 6th International Symposium on Environmental Degradation of Materials in Nuclear Power Systems—Water Reactors, San Diego, CA, USA, 1–5 August 1993; pp. 657–665.
9. Scott, P.M. An Overview of Internal Oxidation as a Possible Explanation of Intergranular Stress Corrosion Cracking of Alloy 600 in PWRs. In Proceedings of the 9th International Symposium on Environmental Degradation of Materials in Nuclear Power Systems—Water Reactors, Newport Beach, CA, USA, 1–5 August 1999; pp. 3–12.
10. Chêne, C. Stress Corrosion Cracking and Hydrogen Embrittlement. In *Stress Corrosion Cracking of Nickel-Based Alloys in Water-Cooled Nuclear Reactors*; Féron, D., Staehle, R.W., Eds.; Elsevier: Amsterdam, The Netherlands, 2016; p. 295. ISBN 978-0-08-100062-5.
11. Simonetti, S.; Lanz, C.; Brizuela, G. Hydrogen Embrittlement of a Fe-Cr-Ni Alloy: Analysis of the Physical and Chemical Processes in the Early Stage of Stress Corrosion Cracking. *Solid State Sci.* **2013**, *15*, 137–141. [CrossRef]
12. Attanasio, S.A.; Fish, J.S.; Wilkening, W.W.; Rosecrans, P.M.; Morton, D.S.; Was, G.S.; Yi, Y. Measurement of the Fundamental Parameters for the Film-Rupture/Oxidation Mechanism—The Effect of Chromium. In Proceedings of the 9th International Symposium on Environmental Degradation of Materials in Nuclear Power Systems—Water Reactors, Newport Beach, CA, USA, 1–5 August 1999; pp. 49–56.
13. Scott, P.M.; Benhamou, C. An Overview of Recent Observations and Interpretations of IGSCC in Nickel Base Alloys in PWR Primary Water. In Proceedings of the 10th International Conference on Environmental Degradation of Materials in Nuclear Power System—Water Reactors, Lake Tahoe, NV, USA, 5–9 August 2001.
14. Fyfitch, S. xLPR Initiation Model Calibration Work. In Proceedings of the Alloy 690/52/152 PWSCC Research Collaboration Meeting, Tampa, FL, USA, 1–3 December 2015.
15. *Alternative Examination Requirements for PWR Reactor Vessel Upper Heads with Nozzles Having Pressure-Retaining Partial-Penetration Welds Section XI, Division 1*; ASME BPVC Cass N-729-1; ASME: New York, NY, USA, 2006.
16. Economy, G.; Jacko, R.J.; Pement, F.W. IGSCC Behavior of Alloy 600 Steam Generator Tubing in Water or Steam Tests Above 360 °C. *Corrosion* **1987**, *43*, 727–734. [CrossRef]
17. DJang, Y.; Watkins, T.R.; Kozaczek, K.J.; Hubbard, C.R.; Cavin, O.B. Surface Residual Stresses in Machined Austenitic Stainless Steel. *Wear* **1996**, *194*, 168–173.
18. Hänninen, H.; Toivonen, A.; Saukkonen, T.; Brederholm, A.; Aaltonen, P.; Ehrnstén, U. EAC Crack Initiation in Nickel-Based Dissimilar Metal Welds Using Doped Steam Test. In Proceedings of the 14th International Conference on Environmental Degradation of Materials in Nuclear Power Systems—Water Reactors, Virginia Beach, VA, USA, 23–27 August 2009; pp. 333–342.
19. Crawford, D.C.; Was, G.S. The Role of Grain Boundary Misorientation in Intergranular Cracking of Ni-16Cr-9Fe in 360 °C Argon and high-Purity Water. *Metall. Trans. A* **1992**, *23*, 1195–1206. [CrossRef]
20. Was, G.S.; Thaveeprungsriporn, V.; Crawford, D.C. Grain Boundary Misorientation Effects on Creep and Cracking in Ni-Based Alloys. *JOM* **1998**, *50*, 44–49. [CrossRef]
21. Gertsman, V.Y.; Bruemmer, S.M. Stud of Grain Boundary Character along Intergranular Stress Corrosion Crack Paths in Austenitic Alloys. *Acta Mater.* **2001**, *49*, 1589–1598. [CrossRef]
22. Panter, J.; Viguier, B.; Cloue, J.M.; Foucault, M.; Combrade, P.; Andrieu, E. Influence of Oxide Films on Primary Water Stress Corrosion Cracking Initiation of Alloy 600. *J. Nucl. Mater.* **2006**, *348*, 213–221. [CrossRef]
23. Combrade, P.; Scott, P.M.; Foucault, M.; Andrieu, E.; Marcus, P. Oxidation of Ni Base Alloys in PWR Water: Oxide Layers and Associated Damage to the Base Metal. In Proceedings of the 12th International Conference on Environmental Degradation of Materials in Nuclear Power System—Water Reactors, Salt Lake City, UT, USA, 14–18 August 2005; pp. 883–890.

24. Lindsay, J.; Scenini, F.; Zhou, X.; Bertali, G.; Cottis, R.A.; Bruke, M.G.; Carrette, F.; Vaillant, F. Characterisation of Stress Corrosion Cracking and Internal Oxidation of Alloy 600 in High Temperature Hydrogenated Steam. In Proceedings of the 16th International Conference on Environmental Degradation of Materials in Nuclear Power System—Water Reactors, Asheville, NC, USA, 11–15 August 2013.
25. Persaud, S.Y.; Korinek, A.; Huang, J.; Botton, G.A.; Newman, R.C. Internal Oxidation of Alloy 600 Exposed to Hydrogenated Steam and the Beneficial Effects of Thermal Treatment. *Corros. Sci.* **2014**, *86*, 108–122. [CrossRef]
26. Bertali, G.; Scenini, F.; Burke, M.G. The Effect of Residual Stress on the Preferential Intergranular Oxidation of Alloy 600. *Corros. Sci.* **2016**, *111*, 494–507. [CrossRef]